Brain, Behavior, and Immunity 116 (2024) 203–215

Contents lists available at ScienceDirect

Brain Behavior and Immunity

journal homepage: www.elsevier.com/locate/ybrbi

Myostatin and CXCL11 promote nervous tissue macrophages to maintain osteoarthritis pain

Christian Martin Gil [a], Ramin Raoof [a], Sabine Versteeg [a], Hanneke L.D.M. Willemen [a], Floris P.J.G. Lafeber [b,c], Simon C. Mastbergen [b,c], Niels Eijkelkamp [a,*]

[a] Center for Translational Immunology, University Medical Center Utrecht, Utrecht University, Utrecht, the Netherlands
[b] Department of Rheumatology and Clinical Immunology, University Medical Center Utrecht, Utrecht University, Utrecht, the Netherlands
[c] Regenerative Medicine Center, University Medical Center Utrecht, Utrecht University, Utrecht, the Netherlands

A B S T R A C T

Pain is the most debilitating symptom of knee osteoarthritis (OA) that can even persist after total knee replacement. The severity and duration of pain do not correlate well with joint tissue alterations, suggesting other mechanisms may drive pain persistence in OA. Previous work identified that macrophages accumulate in the dorsal root ganglia (DRG) containing the somas of sensory neurons innervating the injured knee joint in a mouse OA model and acquire a M1-like phenotype to maintain pain. Here we aimed to unravel the mechanisms that govern DRG macrophage accumulation and programming. The accumulation of F4/80$^+$iNOS$^+$ (M1-like) DRG macrophages was detectable at day 3 after mono-iodoacetate (MIA)-induced OA in the mouse. Depletion of macrophages prior to induction of OA resolved pain-like behaviors by day 7 without affecting the initial development of pain-like behaviors. Analysis of DRG transcript identified CXCL11 and myostatin. CXCL11 and myostatin were increased at 3 weeks post OA induction, with CXCL11 expression partially localized in satellite glial cells and myostatin in sensory neurons. Blocking CXCL11 or myostatin prevented the persistence of OA pain, without affecting the initiation of pain. CXCL11 neutralization reduced the number of total and F4/80$^+$iNOS$^+$ DRG macrophages, whilst myostatin inhibition diminished the programming of F4/80$^+$iNOS$^+$ DRG macrophages. Intrathecal injection of recombinant CXCL11 did not induce pain-associated behaviors. In contrast, intrathecal myostatin increased the number of F4/80$^+$iNOS$^+$ DRG macrophages concurrent with the development of mechanical hypersensitivity that was prevented by macrophages depletion or CXCL11 blockade. Finally, myostatin inhibition during established OA, resolved pain and F4/80$^+$iNOS$^+$ macrophage accumulation in the DRG. In conclusion, DRG macrophages maintain OA pain, but are not required for the induction of OA pain. Myostatin is a key ligand in neuro-immune communication that drives the persistence of pain in OA through nervous tissue macrophages and represent a novel therapeutic target for the treatment of OA pain.

1. Introduction

Osteoarthritis (OA) is a highly prevalent chronic joint disease with increasing prevalence due to the aging and obese world population (Allen, Thoma, & Golightly, 2022; Bijlsma, Berenbaum, & Lafeber, 2011; Safiri et al., 2020). Pain is the primary symptom of OA causing disability and a substantial socioeconomic burden (Neogi, 2013). Current treatments against OA pain are not effective, and some, such as opioids, are associated with long-term adverse effects (Suzuki et al., 1987). Clinical findings show that pain in OA does not correlate well with radiographic damage in the affected joint (Ostojic et al., 2019; Trouvin & Perrot, 2018). Moreover, in patients with a likely neuropathic component, as determined with the painDETECT questionnaire, local and overall joint damage appears to not be the main cause of pain and disability (van Helvoort et al., 2021). Importantly, pain persists in 44 % of OA patients after total knee replacement (Wylde et al., 2011), suggesting that there must be mechanisms other than the local knee joint injury that contribute to OA pain.

At the early stages of OA, pain is thought to be initiated by the activation and sensitization of nociceptive fibers because of pathological changes in the injured joint (Fingleton et al., 2015; Steen Pettersen et al., 2019). However, at later stages central mechanisms also contribute to OA pain (Gwilym et al., 2009; Lluch et al., 2018; Pinto, Lima, & Tavares, 2007). Recently, it has become clear that macrophages have important functions in the regulation of pain. Macrophages with a tissue-healing phenotype (M2-like) attenuate or even actively resolve pain in different rodent models of pain (Raoof, Willemen, & Eijkelkamp, 2018; van der Vlist et al., 2022). Conversely, in animal models of chronic pain, including OA, macrophages with an inflammatory (M1-like) phenotype accumulate in the DRG and contribute to persistent pain (Miller et al., 2012; Raoof et al., 2021; Simeoli et al., 2017). As example, reducing F4/80$^+$iNOS$^+$ (M1-like) macrophages in the DRG, or injecting F4/80$^+$CD206$^+$ (M2-like) macrophages intrathecally, reduced pain-associated behaviors in a rodent model of OA (Raoof et al., 2021).

* Corresponding author at: Lundlaan 6, 3584 EA, Utrecht, the Netherlands.
E-mail address: N.Eijkelkamp@umcutrecht.nl (N. Eijkelkamp).

https://doi.org/10.1016/j.bbi.2023.12.004
Received 27 December 2022; Received in revised form 22 November 2023; Accepted 4 December 2023
Available online 7 December 2023

Overall, these data suggest that the phenotype of macrophages affects their regulatory functions within the nervous system. However, until now it remains unknown how macrophages are engaged in the DRG during OA to maintain pain.

Therefore, we assessed the neuro-immune mechanisms in OA that govern DRG macrophage accumulation and their programming into pro-algesic macrophages.

2. Material and methods

2.1. Animals

All experiments comply with the ARRIVE guidelines, were performed in accordance EU Directive 2010/63/EU for animal experiments and were approved by the local experimental animal welfare body and the national Central Authority for Scientific Procedures on Animals (CCD, license numbers AVD115002015323 and AVD11500202010805).

Adult (age 8–15 weeks) male and female C57BL/6J or $Lysm^{cre/+}$ x $Csf1r^{DTR/+}$ (Cat# 024046, Jackson laboratories) (MM^{dtr}) in a C57Bl/6 background were used and maintained in the animal facility of the University of Utrecht.

Mice were housed in groups under a 12:12 h light/dark cycle, with food and water available *ad libitum*. The cages contained environmental enrichments including tissue papers and shelter. To minimize bias, animals were randomly assigned before the start of experiment using RandoMice. We used baseline mechanical sensitivity, sex and age as factor to equally distribute between groups. Before each experiment the number of mice required was calculated using GPower with an effect size of 1.5–2, power of 80–90 %, and an alpha of 5 % (corrected for multiple testing when needed).

2.2. OA pain model

Mice received an intra-articular injection of 10 μl mono-iodoacetate (MIA; 10 % w/v; Sigma-Aldrich) in one knee joint (ipsilateral) and 10 μl sterile saline (0.9 %) in the other knee joint (contralateral) under isoflurane anesthesia. Knee joints were flexed at a 90° angle, and MIA or sterile saline was injected with a 30-gauge needle (Pitcher, Sousa-Valente, & Malcangio, 2016).

2.3. Pain-associated behavioral tests

1–2 weeks prior to the start of experiments, mice were first acclimatized to the testing environment by placing them in the test environment during 1 h. At least 3 baseline measures were performed at different days during one week before starting the experiment, with the last one at the day of the start of the experiment. Experiments were performed in the same room and same test set-up over the duration of the experiment. Involved experimenters were well trained to perform the assays and were blinded for the experimental groups and genotypes.

Table 1
Antibodies used for flow cytometry.

Target	Fluorophore	Catalog	Clone	Supplier	Dilution
Fixable Viability Dye eFluor 506	BV-510	15,560,607	N.A.	invitrogen eBioscience	1:1000
CD45	APC-ef780	47–0451-80	30-F11	eBioscience	1:600
CD11b	PerCP-Cy5.5	101227(8)	M1/70	BioLegend	1:600
F4/80	FITC	123,108	BM8	BioLegend	1:600
Ly6G	BV-785-A	127,645	1A8	BioLegend	1:300
iNOS	APC	17–5920-80	CXNFT	eBioscience	1:240
CD206	BV650	141,723	C068C2	eBioscience	1:120

To avoid variation, always the same experimenter performed pain behavioral tests in each experiment. Mice were put into the testing environment (von Frey) at least 30 min before performing measurements with the experimenter present in the same room.

Mechanical thresholds were assessed in both hind paws using the von Frey test (Stoelting, Wood Dale, IL, US) with the up-and-down method to determine the 50 % threshold. In short, von Frey filaments were applied for 5 s to the plantar surface of the paw. After applying the first filament (0.4 g), in case of a non-response the next filament with a higher force was used. In case of a response, the next lower force filament was used. A minimum of 30 s between the application of filaments was taken. Four readings were obtained after the first change of direction. Von Frey filaments were applied perpendicularly, smoothly, without moving the filaments horizontally during application. If the response was ambiguous, the measurement was repeated at least one minute later.

Changes in weight bearing were evaluated using the dynamic weight bearing (DWB) apparatus (Bioseb, Vitrolles, France) and the following parameters were used for the analysis: 1) low weight threshold of 0.5 g, 2) high weight threshold of 1 g, 3) surface threshold of 2 cells and 4) minimum 5 images (0.5 s) for stable segment detections. The device consists of a small Plexiglas chamber (11.0 x 19.7 x 11.0 cm) with a sensor mat containing pressure transducers. The system records the average weight that each limb exerts on the floor. Mice were placed in the chamber at least 1 min prior to starting the measurements and were allowed to move freely within the chamber. Each mouse was recorder for period of 5 min. A camera at the top of the enclosure was used to record all movements to ensure accurate validation of the position of the mouse by the experimenter. The relative weight bearing of the affected paw (ipsilateral paw) was expressed as ratio between body weight bore on ipsilateral paw divided by body weight bore on the unaffected paw (contralateral paw).

2.4. Depletion of monocytes and macrophages

To deplete monocytes and macrophages *in vivo*, MM^{dtr} mice received a first intraperitoneal injection of 20 ng/g body weight diphtheria toxin (DT; Sigma-Aldrich) followed by daily intraperitoneal injections of 4 ng/g body weight DT at all subsequent days as described previously (Schreiber et al., 2013).

2.5. Neutralization of CXCL11 and myostatin

To neutralize CXCL11 and myostatin *in vivo*, mice received daily intrathecal injections of anti-CXCL11 IgG (Mouse CXCL11/I-TAC IgG2A Antibody, Cat# MAB572, R&D) and polyclonal anti-myostatin IgG (Human/Mouse/Rat GDF-8/Myostatin Antibody, Cat# AF788, R&D) antibodies. Rat IgG2A Isotype Control (Cat# MAB006, R&D) was used as anti-CXCL11 control, and normal polyclonal Goat IgG Control (Cat# AB-108-C, R&D) as polyclonal anti-myostatin control.

2.6. Monocyte isolation and in vitro differentiation into macrophages

For monocyte-derived macrophage generation, $10x10^6$ bone-marrow cells were seeded in a 75 cm^2 non-treated tissue culture flasks (VWR, Radnor, PA) for 7 days in macrophage medium (High-glucose Dulbecco's Modified Eagle medium (DMEM; Cat# 31966–021, GIBCO) and DMEM/F12 (Cat# 31331–028, GIBCO) (1:1)), supplemented with 30 % L929 cell-conditioned medium, 10 % fetal bovine serum (FBS; Cat# 10270–106, GIBCO), 1 % Penicillin/Streptomycin (GIBCO) and 1 % L-Glutamine (200 mM, ThermoFisher).

To obtain L929 cell-conditioned medium, $10x10^6$ L929 (ATCC CCL-1) cells were seeded in a 75 cm^2 flask with cell culture-medium supplemented with 1 % non-essential amino acids (Sigma-Aldrich) for one week. L929 cells were passaged to a 162 cm^2 flask with 50 ml medium and after a week the supernatants were collected and filtered through a 0.2-μm filter and stored at −20 °C (L929-derived M−CSF).

Table 2
Antibodies used for immunofluorescence.

Target	Fluorophore	Catalog	Clone	Supplier	Dilution
Myostatin	None	AB3239-I	Polyclonal rabbit	Sigma-Aldrich	1:100
CXCL11	None	BS-2552R	Polyclonal rabbit	Bioss	1:100
Isotype control	None	31,235	Control	ThermoFisher	1:100
B3-Tubulin	None	ab41489	Polyclonal chicken	abcam	1:1000
FABP7	None	AF3166	Polyclonal goat	R&D	1:1000
GFAP	None	BM2287	Monoclonal mouse	OriGene	1:500
Anti-chicken	AF-488	A11039	Goat	ThermoFisher	1:500
Anti-chicken	AF-594	A11012	Goat	ThermoFisher	1:500
Anti-goat	AF-488	A11055	Donkey	ThermoFisher	1:500
Anti-mouse	AF-594	A11005	Goat	ThermoFisher	1:500
Anti-rabbit	AF-488	A11008	Goat	ThermoFisher	1:500
Anti-rabbit	AF-750	A21039	Goat	ThermoFisher	1:500

2.7. Adoptive transfer of macrophages

Cells were injected intrathecally (30,000 cells/5 μl per mouse) (van der Vlist et al., 2022) under light isoflurane anesthesia as described previously (Eijkelkamp et al., 2010; Hylden & Wilcox, 1980).

2.8. Flow cytometry analysis

DRG (L3–L5) or spinal cord were collected to analyze infiltrating immune cells. In brief, tissues were gently minced and dissociated at 37 °C for 30 min with an enzyme cocktail (1 mg collagenase type I with 0.5 mg trypsin in 1 ml DMEM; Sigma-Aldrich). Cells were stained with various combinations of fluorochrome-labeled antibodies (Table 1). Absolute number of cells was calculating using counting beads (Count-Bright™ Absolute Counting Beads, for flow cytometry, Cat# C36950, ThermoFisher). A defined set of counting beads was added to the DRG cell suspension. Based on the number of measured beads during flow cytometry the total number of cells in the DRG cell suspension was calculated.

2.9. Immunofluorescent stainings

Mice were killed by cervical dislocation and DRG were collected. For some experiments, the retrograde marker Wheat Germ Agglutinin (WGA) was injected intra-articular 48 h prior to killing the mice (WGA-594, Cat.# W11262, ThermoFisher) to identify sensory neurons innervating the knee joint.

Tissues were post-fixed in 4 % paraformaldehyde (PFA) overnight, cryoprotected in 30 % (w/v) sucrose overnight, embedded in optimal cutting temperature (OCT) compound (Sakura, Zoeterwoude, the Netherlands) and frozen at −80 °C.

Cryosections (10 μm) of lumbar DRG (L3-L5) were cut on a cryostat (Leica CM3050 S Cryostat), post-fixed in 4 % PFA during 5 min and stained with primary antibodies overnight at 4 °C, followed by 2 h incubation with fluorescent-tagged secondary antibodies (Table 2). Nuclei were counterstained with or without 4,6-diamidino-2-phenylindole (DAPI). Immunostaining images were captured with an Olympus IX83 microscope using identical exposure times for all slides within one experiment.

2.10. RNA isolation and RT

Total RNA was isolated from freshly isolated DRG (L3-L5) using TRIzol and RNeasy mini kit (QIAGEN, Hilden, Germany). cDNA was synthesized using iScript reverse transcription supermix, according to manufacture protocol (Bio-Rad, Hercules, CA).

2.11. PCR array

Mature RNA was isolated as described above. RNA quality was determined using a spectrophotometer and was reverse transcribed using a cDNA conversion kit. cDNA from 5 mice belonging to the same group were pooled. The cDNA was used on the real-time RT^2 Profiler PCR Array (Cat# PAMM-150Z, QIAGEN) in combination with RT^2 SYBR® Green qPCR Mastermix (Cat# 330529, QIAGEN). Fold change/regulation were calculated using delta delta CT method, in which delta CT is calculated between gene of interest and an average of reference genes, followed by delta-delta CT calculations (delta CT (Test Group)-delta CT (Control Group)). Fold Change is then calculated using 2^(-delta delta CT) formula. Samples passed PCR Array Reproducibility, RT Efficiency and Genomic DNA Contamination quality checks. For normalization, CT values of β-actin, β2-microglobulin, GAPDH, β-glucuronidase and HSP 90- β expression were used to calculate the average of reference genes.

2.12. Real-time RT-PCR

Quantitative real-time PCR reactions were performed using a QuantStudio 3 (ThermoFisher) following the manufacturer's instructions. We used 1–5 ng cDNA input per qPCR reaction and used the mean of 18S rRNA, β2-microglobulin and TBP expression as reference. Primers used are included in Table 3.

2.13. Statistical analysis

All data are presented as mean ± SD and were analyzed with GraphPad Prism version 9.3 using unpaired two-tailed t-tests, one-way or two-way ANOVA, or as appropriate two-way repeated-measures ANOVA, followed by post hoc analysis. The used post hoc analyses are indicated in each figure legend. Data are represented as mean ± SD. A p

Table 3
Primers used for Real-Time RT-PCR.

Target	Forward	Reverse
CXCL11	GCTGCTGAGATGAACAGGAA	CCCTGTTTGAACATAAGGAAGC
Myostatin	CAGCCTGAATCCAACTTAGG	TCGCAGTCAAGCCCAAAGTC
IL-6	CTAATTCATATCTTCAACCAAGAGG	TGGTCCTTAGCCACTCCTTC
18S rRNA	GTAACCCGTTGAACCCCATT	CCATCCAATCGGTAGTAGCG
β2-microglobulin	ATTCACCCCCACTGAGACTG	TGCTATTTCTTTCTGCGTGC
TBP	CCTTGTACCCTTCACCAATGAC	ACAGCCAAGATTCACGGTAGA

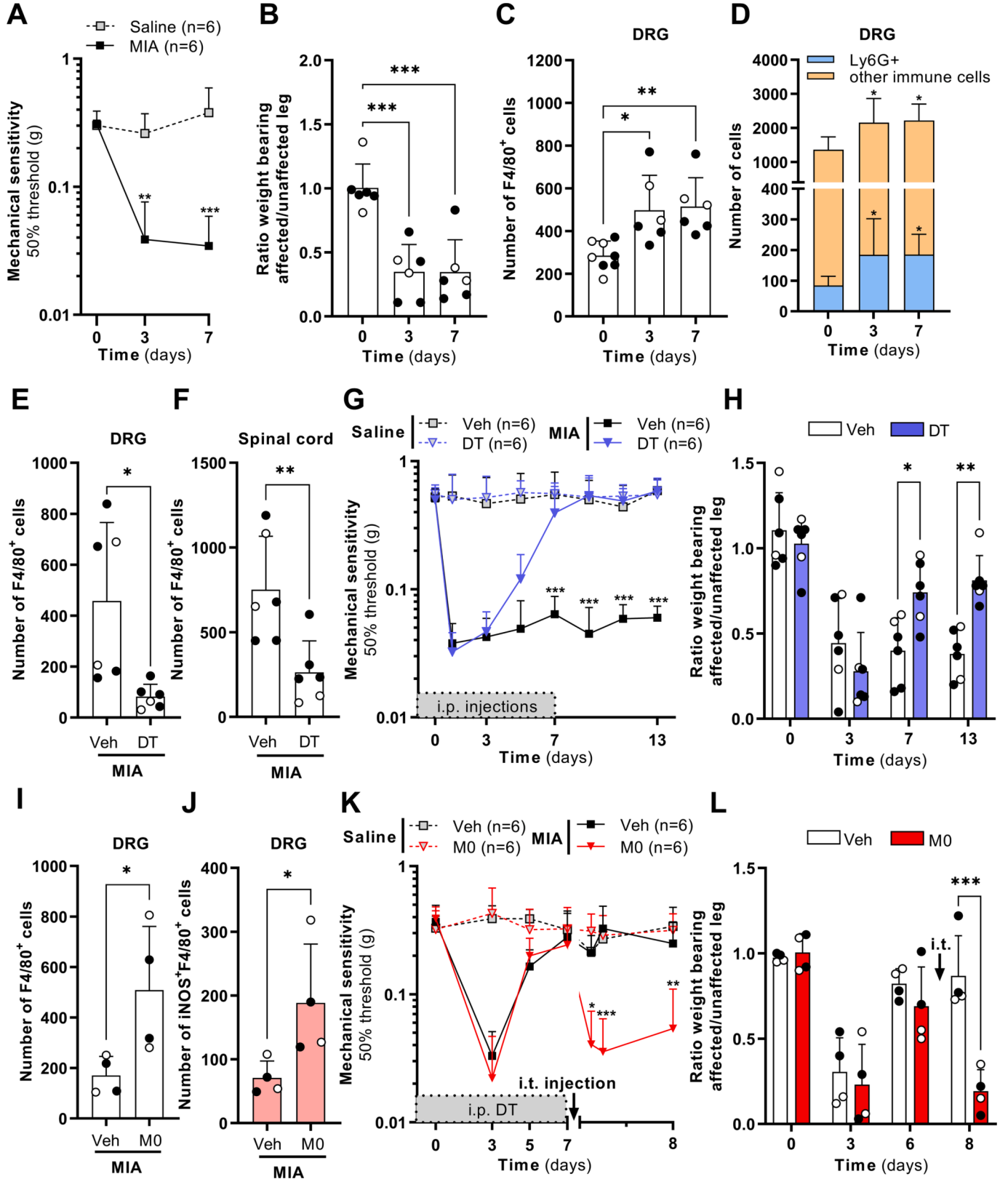

(caption on next page)

Fig. 1. DRG macrophages maintain pain but are not involved in the initiation of OA pain. Course of (**A**) mechanical hypersensitivity and (**B**) weight bearing of ipsilateral hind paw after an unilateral intra-articular injection of MIA. As control, mice received saline in the contralateral knee. Two-way ANOVA with Sidak's post hoc. Flow cytometry of a cell suspension of ipsilateral lumbar DRG (L3–L5) of (**C**) $CD45^+CD11b^+Ly6G^-F4/80^+$ macrophages, (**D**) $CD45^+Ly6G^+$ neutrophils and other immune cells defined as $CD45^+Ly6G^-CD11b^-F4/80^-$ comparing day 0 with day 3 and 7 days after MIA injection. One-way ANOVA with Dunett's post hoc. To deplete monocytes and macrophages, mice received daily intraperitoneal DT injections starting one day prior intra-articular injection of MIA. Flow cytometry analysis of a cell suspension showing total $CD45^+CD11b^+Ly6G^-F4/80^+$ macrophages in (**E**) ipsilateral lumbar DRG (L3-L5) and (**F**) lumbar section from spinal cord of MM^{dtr} mice injected intraperitoneally with DT or saline at day 7 after injection with MIA. Gating strategy is displayed in Fig. S1. Unpaired two-tailed *t*-test. Course of (**G**) mechanical hypersensitivity and (**H**) weight bearing on ipsilateral hind paw in MM^{dtr} mice injected daily with DT or vehicle. Two-way ANOVA with Dunnet's post hoc comparing vehicle and DT treatments at each time point. MM^{dtr} mice injected with DT starting one day prior intra-articular injection of MIA in the ipsilateral knee and saline in the contralateral knee, received intrathecal exogenous macrophages or vehicle at day 7. Analysis of the number of (**I**) total $CD45^+CD11b^+Ly6G^-F4/80^+$ macrophages and (**J**) $CD45^+CD11b^+Ly6G^-F4/80^+iNOS^+$ macrophages in the ipsilateral lumbar DRG (L3–L5) at 24 h after this intrathecal injection. Unpaired two-tailed *t*-test. Course of (**K**) mechanical hypersensitivity and (**L**) weight bearing on ipsilateral hind paw in MM^{dtr} mice injected with DT starting one day prior unilateral intra-articular injection of MIA. At day 7, mice received intrathecal exogenous macrophages or vehicle. Two-way ANOVA with Sidak's post hoc. Open dots (○) represent males and closed dots represent females (●) in column graphs from panels B, C, E, F, H, I, J and L. A p-value less than 0.05 was considered statistically significant and each significance is indicated with *$p < 0.05$, **$p < 0.01$, ***$p < 0.001$.

value less than 0.05 was considered statistically significant.

2.14. Data availability

All data are available in the article or in Supplementary materials. Raw data and materials are available on reasonable request. Some materials used in this manuscript are subject to a material transfer agreement.

3. Results

3.1. $F4/80^+iNOS^+$ macrophages accumulate in the DRG during early OA and maintain pain

Knee joint damage was induced by an unilateral intra-articular injection of MIA (10 % w/v). At day 3 after MIA-induced OA, mice showed signs of pain-like behaviors such as mechanical hypersensitivity as assessed with von Frey test, and weight bearing deficits assessed with dynamic weight bearing (Fig. 1A/B). Earlier findings show that macrophages are at least present from one week up to 4 weeks after induction of OA with MIA (Raoof et al., 2021). To investigate whether DRG macrophages accumulate earlier during initiation of OA pain, the L3–L5 DRG that contain the somas of sensory neurons innervating the knee joint, were analyzed using flow cytometry (Fig. S1). Macrophages were gated based on $CD45^+Ly6G^-CD11b^+F4/80^+$, further referred to as $F4/80^+$ DRG macrophages. The number of $F4/80^+$ DRG macrophages was increased at day 3 and day 7 after intra-articular MIA injection (Fig. 1C). $Ly6G^+$ neutrophils, gated based on $CD45^+Ly6G^+$, and other immune cell numbers, gated based on $CD45^+Ly6G^-CD11b^-F4/80^-$, were also significantly increased in the DRG at these time points (Fig. 1D).

Next, we selectively depleted monocytes and macrophages by daily intraperitoneal injections of diphtheria toxin (DT) in $Lysm^{cre/+}$ x $Csf1r^{DTR/+}$ mice (Schreiber et al., 2013), referred to as "MM^{dtr},". Daily intraperitoneal DT injection reduced the number of $F4/80^+$ macrophages in the DRG and spinal cord compared to saline injected MM^{dtr} mice at day 7 after injection of MIA (Fig. 1E/F). In macrophage-depleted mice, MIA-induced mechanical hypersensitivity and weight bearing deficits were indistinguishable from non-depleted mice until day 7. However, at day 7 after MIA injection, macrophages-depleted mice had progressively resolved from mechanical hypersensitivity and deficits in weight bearing, and stayed resolved until day 13 after MIA injection, compared to non-depleted mice (Fig. 1G/H).

To further support the role of DRG macrophages to maintain OA pain, 30.000 (van der Vlist et al., 2022), DT resistant, wild type bone marrow-derived macrophages were injected intrathecally into macrophages-depleted MM^{dtr} mice 7 days after MIA injection. Pro-inflammatory, M1-like macrophages were gated based on $CD45^+Ly6G^-CD11b^+F4/80^+iNOS^+$, further referred to as $F4/80^+iNOS^+$ macrophages. Intrathecal injection of bone marrow-derived macrophages resulted in an increase in the number of total $F4/80^+$ macrophages and $F4/80^+iNOS^+$ macrophages in the DRG (Fig I/J). Intriguingly, these macrophages were sufficient to reinstate mechanical hypersensitivity in the ipsilateral paw in macrophage-depleted MM^{dtr} mice, but not in the contralateral paw (Fig. 1K). Similarly, intrathecal macrophages reinstated weight bearing deficits in macrophage-depleted MM^{dtr} mice (Fig. 1L).

3.2. CXCL11 and myostatin expression in the DRG during early OA

To identify which factors may drive the accumulation and programming of macrophages in the DRG during OA we used a PCR array for 96 mouse cytokines and chemokines (Table S1). Analysis of DRG transcript at 3 days after intra-articular MIA injection identified CXCL11, IL-6, IL-18 and myostatin as top 4 of most highly differentially expressed genes. As CXCL11 is known as chemoattractant for monocytes/macrophages (Zeng et al., 2016), and myostatin can inhibit macrophages pro-inflammatory programming in adipose and muscle tissue (Dong et al., 2016), we focused further on these 2 novel mediators as potential targets of interest.

To validate the increase in CXCL11 and myostatin expression, we determined CXCL11 and myostatin mRNA levels in the DRG using qPCR and using a larger experiment. At day 3 after MIA injection, we confirmed that expression of CXCL11 was ~ 1.5 fold higher than controls and myostatin mRNA was increased with ~ 4-fold. At 7 and 21 days after MIA injection, CXCL11 expression did not differ from DRG from control mice. Myostatin mRNA expression was doubled compared to controls at days 7 and 21, but not significant (Fig. 2A/B).

To confirm the increase of CXCL11 and myostatin protein expression in the DRG, we measured CXCL11 and myostatin after immunofluorescent staining of the DRG from control mice and mice at day 3 and 21 after MIA injection. CXCL11 immunofluorescence was increased in the ipsilateral lumbar DRG (L3-L5) compared to the DRG of mice without MIA injection at days 3 and 21 after MIA injection (Fig. 2C). CXCL11 expression appeared to colocalize in part with FABP7 and GFAP (satellite glial cell markers) (Fig. 2D), suggesting satellite glial cells may be a source of CXCL11. Staining with isotype IgG did not give any visible staining (Fig. S2).

Myostatin expression, in contrast, colocalized with β3-tubulin positive cells in the DRG (Fig. 2E), suggesting myostatin is produced within sensory neurons. Anti-myostatin IgG blocked recombinant myostatin did not give any staining (Fig. S3). To quantify neuronal myostatin expression, we binned sensory neurons according to their cross-sectional area. Myostatin expression was increased at day 3 and day 21 in small DRG neurons (0–300 μm^2). In medium (300–600 μm^2) and large (600–2000 μm^2) DRG neurons myostatin expression was increased at day 21, but not day 3 (Fig. 2F). To assess whether the observed changes in myostatin expression occur in neurons innervating the affected knee joint, we injected the retrograde tracer, wheat germ agglutin (WGA) 2 days priors to isolation of DRG. Myostatin fluorescent intensity was

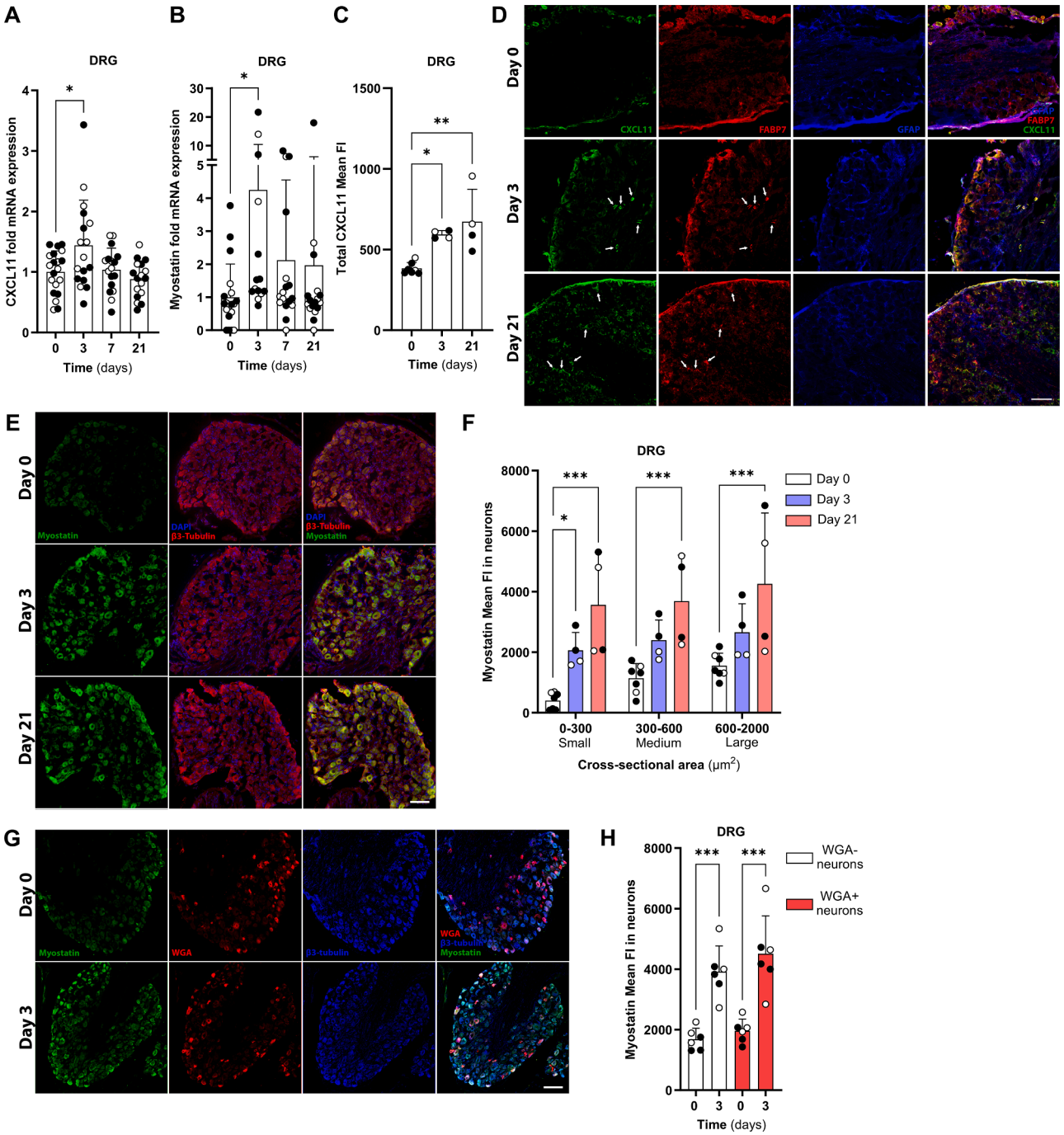

Fig. 2. Increased CXCL11 and myostatin expression in the DRG of mice with OA. (A) CXCL11 and (B) myostatin mRNA expression in ipsilateral lumbar DRG (L3-L5) comparing control mice (day 0) with mice at days 3, 7 and 21 after MIA injection. One-way ANOVA with Dunnett's post hoc. (C) Quantification of CXCL11 signal in the lumbar DRG (L3-L5) from naive mice (day 0) and ipsilateral DRG from mice at days 3 and 21 after MIA injection. One-way ANOVA with Dunnett's post hoc. (D) Example images showing CXCL11, FABP7 and GFAP fluorescence in the DRG from naive mice (day 0) and ipsilateral lumbar DRG (L3-L5) from mice at days 3 and 21 after MIA injection. Control isotype IgG staining is shown in Fig. S2. (E) Example images showing myostatin and β3-Tubulin signal after immunofluorescent staining of ipsilateral lumbar DRG (L3-L5) of naive mice (day 0) and mice at days 3 and 21 after MIA injection. Control anti-myostatin IgG staining where the antibody was blocked with recombinant myostatin (Cat# 120–00, PeproTech) is displayed in Fig. S3. (F) Quantification of myostatin fluorescence in small (0–300 μm^2), medium (300–600 μm^2) and large (0–2000 μm^2) cross-sectional area neurons from lumbar DRG (L3-L5) of naive mice (day 0) and ipsilateral DRG from mice at days 3 and 21 after MIA injection. Two-way ANOVA with Dunnett's post hoc. (G) Mice were injected intra-articular with WGA to identify the somas of sensory neurons innervating the knee joint. Example images of myostatin, WGA and β3-Tubulin fluorescence in the ipsilateral lumbar DRG (L3-L5) of naive mice (day 0) and mice at 3 days after MIA injection. Isotype IgG was used as control and is displayed in Fig. S4. (H) Quantification of myostatin fluorescent signal in WGA- and WGA + sensory neurons in the ipsilateral lumbar DRG (L3-L5) of naive mice (day 0) and mice at day 3 after MIA injection. One-way ANOVA with Tukey's post hoc. Open dots (○) represent males and closed dots represent females (●) in column graphs from panels A, B, C, F and H. A p-value less than 0.05 was considered statistically significant and each significance is indicated with *$p < 0.05$, **$p < 0.01$, ***$p < 0.001$. White arrows in panel D point to the areas where CXCL11 and FABP7 signal colocalize. White scale bars on the bottom right corner of panels D, E and G represents 100 μm.

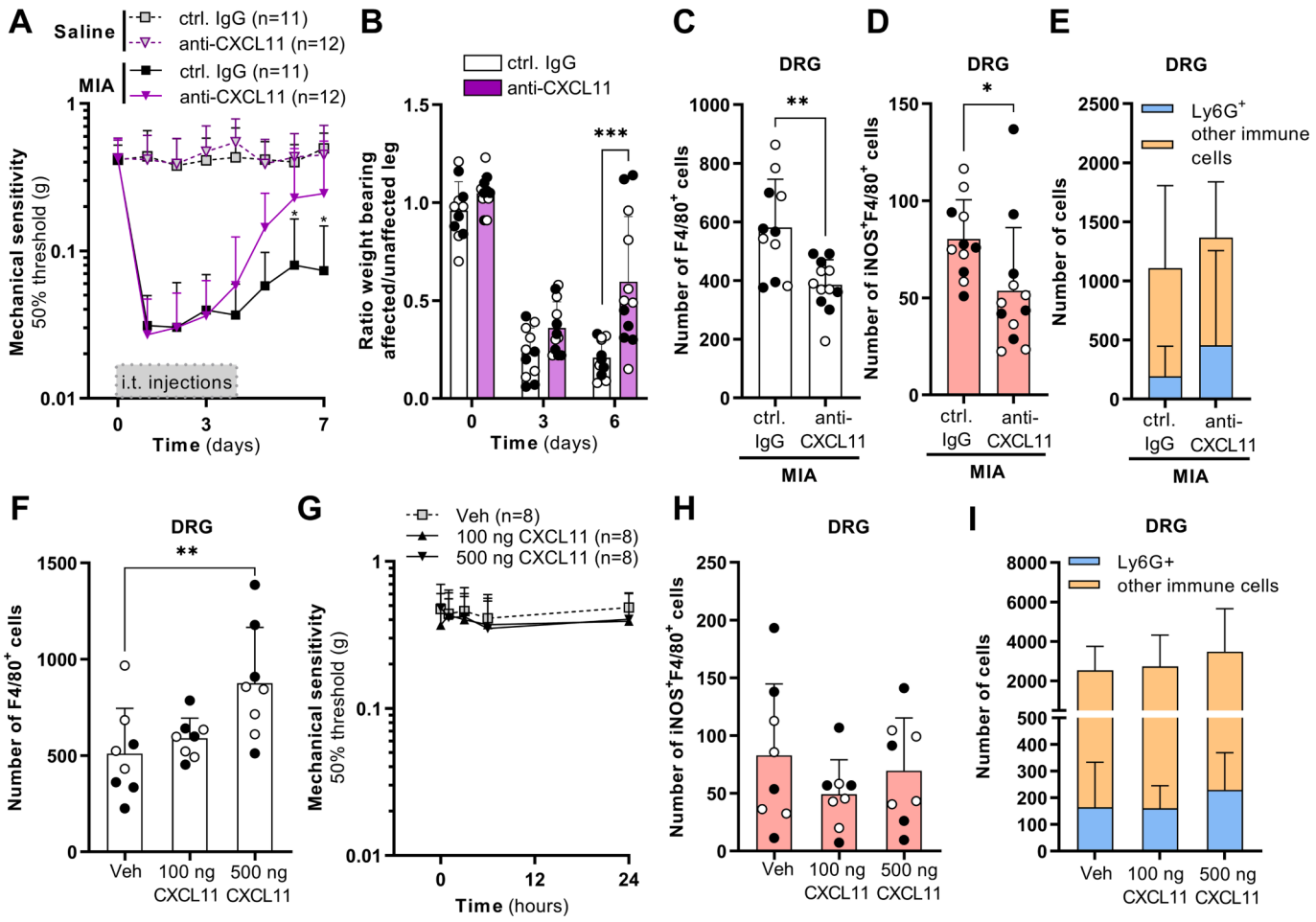

Fig. 3. CXCL11 drives DRG macrophage accumulation in OA, but is not sufficient to induce pain-like behaviors. Course of (**A**) mechanical hypersensitivity and (**B**) weight bearing of ipsilateral hind paw after an unilateral intra-articular MIA injection. Saline was injected into the contralateral knee joint. Anti-CXCL11 (2.5 μg/injection) or control IgG (2.5 μg/injection) were injected intrathecally, daily for 5 days, starting just prior to MIA injection. Two-way ANOVA with Sidak's post hoc. Flow cytometry analysis of the number of (**C**) $CD45^+CD11b^+Ly6G^-F4/80^+$ macrophages, (**D**) $CD45^+CD11b^+Ly6G^-F4/80^+iNOS^+$ macrophages, (**E**) $CD45^+Ly6G^+$ neutrophils and other immune cells defined as $CD45^+Ly6G^-CD11b^-F4/80^-$ in the ipsilateral lumbar DRG (L3–L5) at day 7 after MIA injection. Unpaired two-tailed *t*-test. (**F**) Analysis of the number of total $CD45^+CD11b^+Ly6G^-F4/80^+$ macrophages in left and right side lumbar DRG (L3–L5) at 24 h after intrathecal CXCL11 injection. One-way ANOVA with Dunnett's post hoc. (**G**) Course of mechanical hypersensitivity after intrathecal injection of vehicle, 100 ng or 500 ng of CXCL11 in mice. Two-way ANOVA with Dunnett's post hoc. (**H**) $CD45^+CD11b^+Ly6G^-F4/80^+iNOS^+$ macrophages, (**I**) $CD45^+Ly6G^+$ neutrophils and other immune cells defined as $CD45^+Ly6G^-CD11b^-F4/80^-$ in the left and right side lumbar DRG (L3–L5) at 24 h after intrathecal injection. One-way ANOVA with Dunnett's post hoc. Open dots (○) represent males and closed dots represent females (●) in column graphs from panels B, C, D, F and H. A p-value less than 0.05 was considered statistically significant and each significance is indicated with *$p < 0.05$, **$p < 0.01$, ***$p < 0.001$.

increased in WGA+ neurons compared to naive mice at 3 days after MIA injection. In WGA- sensory neurons, myostatin expression was also increased, indicating myostatin is not only regulated in neurons innervating the knee joint. (Fig. 2G/H; Fig S4 for Isotype control staining).

3.3. Role of CXCL11 in OA pain

To address whether CXCL11 in DRG is required for the persistence of OA pain, we neutralized endogenous CXCL11 by administration of daily intrathecal injections of anti-CXCL11 for five days starting the day of MIA injection. Intrathecal injection of anti-CXCL11 IgG prevented the development of persistent mechanical hypersensitivity and weight bearing deficits compared to mice injected with a control IgG antibody. In contrast, the initiation of OA pain until day 3 was not affected by the inhibition of CXCL11 compared to the control IgG antibody treatment (Fig. 3A/B). Neutralization of CXCL11 reduced the number of $F4/80^+$ macrophages in the DRG (Fig. 3C). In addition, the number of $F4/80^+iNOS^+$ macrophages in the DRG was reduced with 33 % compared to control IgG-treated mice (Fig. 3D). $Ly6G^+$ neutrophils and other immune cells in the DRG remained unaffected after CXCL11 inhibition (Fig. 3E).

Next, we tested whether CXCL11 intrathecal injection is sufficient to induce pain-like behaviors and DRG macrophage accumulation. Intrathecal injection of 100 and 500 ng CXCL11 (Piotrowska et al., 2018) dose dependently increased the number of $F4/80^+$ macrophages in lumbar DRG (Fig. 3F). In contrast, these doses of CXCL11 did not induce mechanical hypersensitivity (Fig. 3G), nor increased the number of $F4/80^+iNOS^+$ macrophages or other immune cells in the DRG (Fig. 3H/I). These data suggest that CXCL11 alone is not sufficient to induce pain-associated behaviors.

3.4. Myostatin maintains OA pain

Next, we assessed the role of myostatin in OA pain by daily intrathecal injections of neutralizing anti-myostatin IgG, starting just prior to intra-articular MIA injection for five days. Anti-myostatin IgG resolved MIA-induced mechanical hypersensitivity starting from day 3, whilst control IgG had no effect. Seven days after MIA injection mechanical

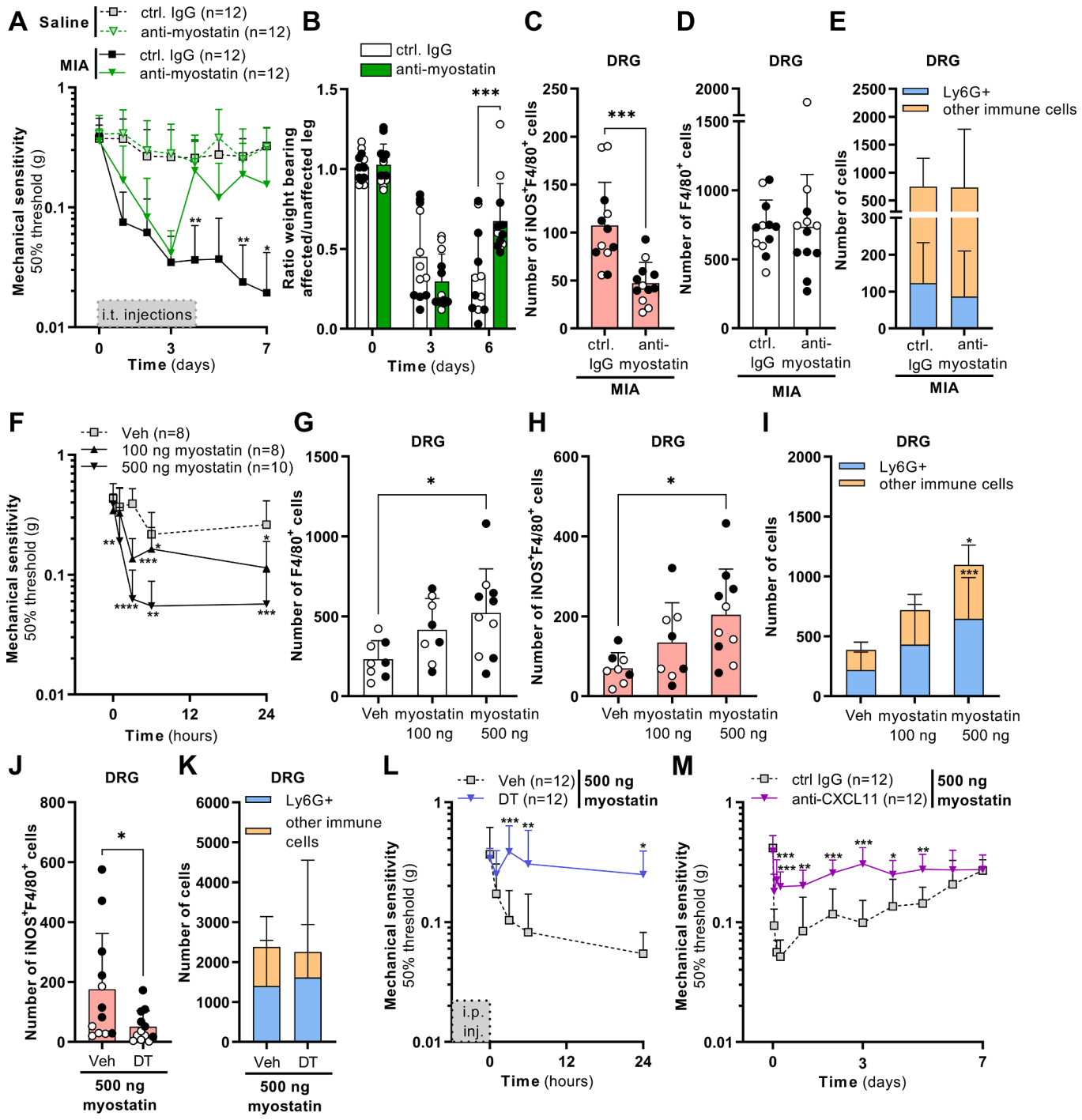

Fig. 4. Myostatin maintains OA pain and is sufficient to induce pain-associated behaviors that require macrophages and CXCL11. Course of (**A**) mechanical hypersensitivity and (**B**) weight bearing of ipsilateral hind paw after an unilateral intra-articular MIA injection. Saline was injected into the contralateral knee joint. Starting just prior to MIA injection, mice received 5 daily intrathecal injections with anti-myostatin IgG (2.5 μg/injection) or control IgG (2.5 μg/injection). Two-way ANOVA with Sidak's post hoc. Flow cytometry analysis of the number of (**C**) total $CD45^+CD11b^+Ly6G^-F4/80^+iNOS^+$ macrophages, (**D**) $CD45^+CD11b^+Ly6G^-F4/80^+$ macrophages, (**E**) $CD45^+Ly6G^+$ neutrophils and other immune cells defined as $CD45^+Ly6G^-CD11b^-F4/80^-$ in the ipsilateral lumbar DRG (L3–L5) at day 7 after MIA injection. Unpaired two-tailed *t*-test. (**F**) Course of mechanical hypersensitivity after intrathecal injection of saline, 100 ng or 500 ng of myostatin in mice. Two-way ANOVA with Dunnett's post hoc. Analysis of the number of (**G**) total $CD45^+CD11b^+Ly6G^-F4/80^+$ macrophages, (**H**) $CD45^+CD11b^+Ly6G^-F4/80^+iNOS^+$ macrophages, (**I**) $CD45^+Ly6G^+$ neutrophils and other immune cells defined as $CD45^+Ly6G^-CD11b^-F4/80^-$ in the left and right side lumbar DRG (L3–L5) at 24 h after intrathecal treatment. One-way ANOVA with Dunnett's post hoc. (**J**) $CD45^+CD11b^+Ly6G^-F4/80^+iNOS^+$ macrophages, (**K**) $CD45^+Ly6G^+$ neutrophils and other immune cells defined as $CD45^+Ly6G^-CD11b^-F4/80^-$ in the left and right side lumbar DRG (L3–L5) from mice injected with DT or saline at 24 h after intrathecal administration of myostatin. Unpaired two-tailed *t*-test. (**L**) Course of mechanical hypersensitivity during the 24 h after intrathecal injection of myostatin, comparing MM^{dtr} mice previously treated with 4 daily intraperitoneal injections of DT compared to saline. Two-way ANOVA with Sidak's post hoc. (**M**) Course of mechanical hypersensitivity after intrathecal injection of myostatin (500 ng) combined with anti-CXCL11 (2.5 μg) or control IgG (2.5 μg). Two-way ANOVA with Sidak's post hoc. Open dots (○) represent males and closed dots represent females (●) in column graphs from panels B, C, D, G, H and J. A p-value less than 0.05 was considered statistically significant and each significance is indicated with *$p < 0.05$, **$p < 0.01$, ***$p < 0.001$.

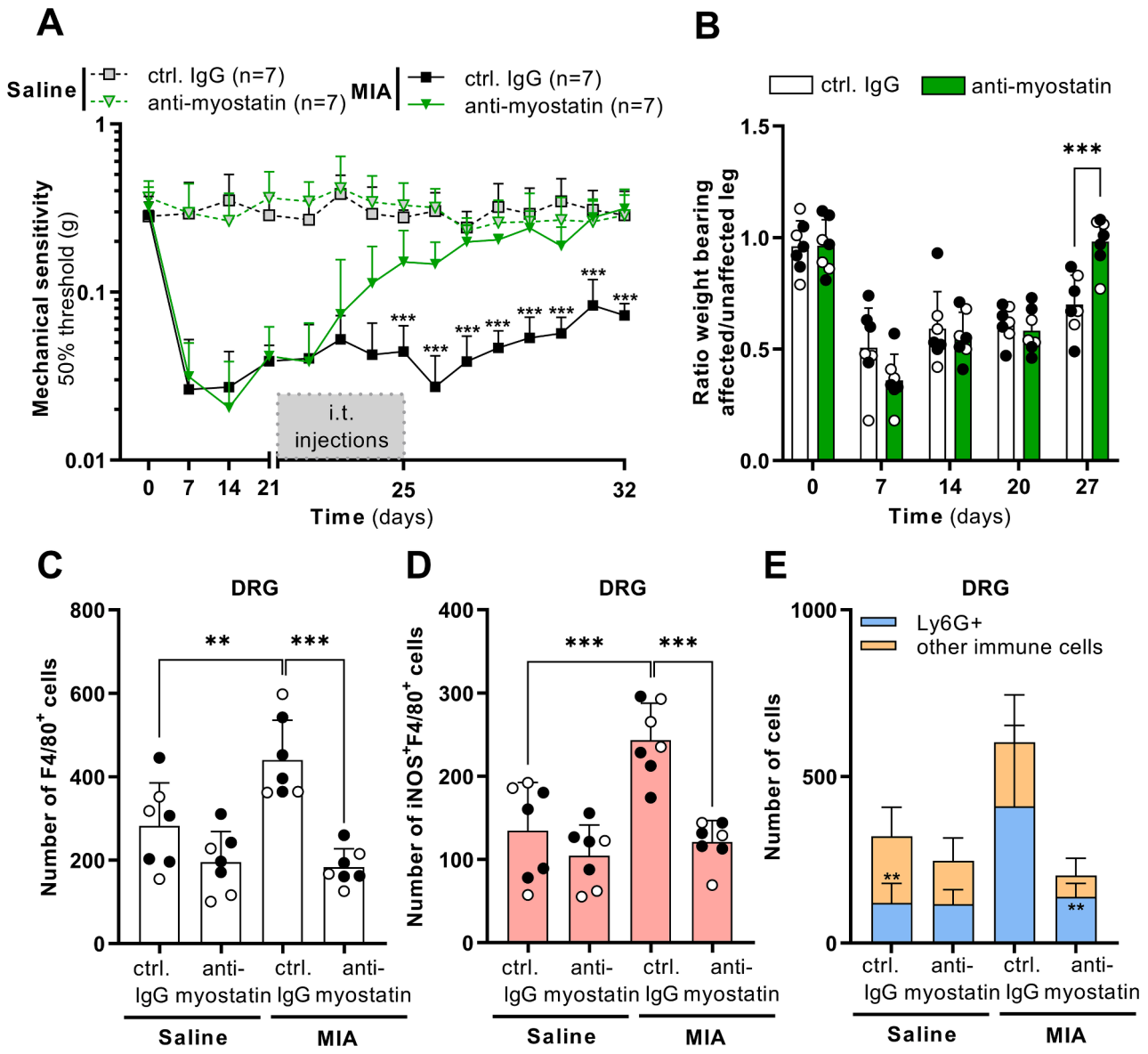

Fig. 5. Myostatin neutralization resolves persistent OA pain. Course of (**A**) mechanical hypersensitivity and (**B**) weight bearing of ipsilateral hind paw after an unilateral intra-articular MIA injection. Saline was injected into the contralateral knee joint. Five daily intrathecal injections of anti-myostatin IgG (2.5 μg/injection) or control IgG (2.5 μg/injection) were administered starting at day 21 after MIA injection. Two-way ANOVA with Sidak's post hoc. Analysis of the number of (**C**) total $CD45^+CD11b^+Ly6G^-F4/80^+$ macrophages, (**D**) $CD45^+CD11b^+Ly6G^-F4/80^+iNOS^+$ macrophages, (**E**) $CD45^+Ly6G^+$ neutrophils and other immune cells defined as $CD45^+Ly6G^-CD11b^-F4/80^-$ in the ipsilateral and contralateral lumbar DRG (L3–L5) at day 32 after MIA injection. One-way ANOVA with Dunnett's post hoc. Open dots (○) represent males and closed dots represent females (●) in column graphs from panels B, C and D. A p-value less than 0.05 was considered statistically significant and each significance is indicated with, $^{**}p < 0.01$, $^{***}p < 0.001$. In panel E, asterisks (*) indicate statistically significant differences in number of Ly6G + neutrophils between MIA compared to saline. No significant differences were found in the number of other immune cells among groups.

hypersensitivity fully resolved in anti-myostatin IgG treated mice (Fig. 4A). Similarly, at day 7 after MIA, weight bearing deficits were normalized in mice that received anti-myostatin IgG (Fig. 4B). Inhibition of myostatin did reduce the number of $F4/80^+iNOS^+$ macrophages in the DRG with 56 % compared to mice treated with a control IgG (Fig. 4C), without affecting the total number $F4/80^+$ macrophages, $Ly6G^+$ neutrophils or other immune cells in the DRG (Fig. 4D/E).

Intrathecal injection of either 100 ng or 500 ng myostatin induced mechanical hypersensitivity within 3 h that persisted for at least 24 h (Fig. 4F). Injection of 500 ng myostatin significantly increased the total $F4/80^+$ macrophages, $F4/80^+iNOS^+$ macrophages, $Ly6G^+$ neutrophils and other immune cells (CD45 + but negative for macrophage and neutrophil markers) number in the DRG compared to the vehicle (Fig. 4G/H/I).

To determine whether myostatin-induced pain requires macrophages, we injected myostatin in monocyte/macrophages-depleted mice. MM^{dtr} mice received 4 daily intraperitoneal injections of DT prior to intrathecal injection of recombinant myostatin. Depletion of macrophages prior intrathecal injection of myostatin completely prevented myostatin-induced increase in $F4/80^+iNOS^+$ DRG macrophages, while $Ly6G^+$ neutrophils and other immune cells remained unaffected (Fig. 4J/K). Importantly, macrophages depletion completely prevented myostatin-induced mechanical hypersensitivity (Fig. 4L).

Because myostatin neutralization reduced mechanical sensitivity earlier in time than CXCL11 neutralization (Fig. 3A vs 4A), we hypothesized that myostatin may be upstream of CXCL11. To test this hypothesis, we intrathecally injected myostatin whilst neutralizing CXCL11 with anti-CXCL11. Administration of anti-CXCL11 together

with myostatin significantly reduced the development of myostatin-induced pain compared to mice injected intrathecally with myostatin and control IgG antibody (Fig. 4M).

3.5. Inhibition of myostatin resolves persistent OA pain

To assess if targeting myostatin is a therapeutic approach to treat persistent OA pain, mice received daily intrathecal injections during five days with neutralizing anti-myostatin IgG starting at 21 days after induction of OA. Anti-myostatin IgG resolved MIA-induced mechanical hypersensitivity from 3 days onwards after starting the intrathecal treatment. At day 27, mechanical hypersensitivity had fully resolved and weight bearing deficits were normalized in mice that had received anti-myostatin IgG (Fig. 5A/B). At day 32, the number of total F4/80$^+$ macrophages, F4/80$^+$iNOS$^+$ macrophages, Ly6G$^+$ neutrophils and other immune cells in the DRG had fully normalized in anti-myostatin IgG treated mice (Fig. 5C/D/E).

4. Discussion

In this study we focused on the neuro-immune mechanisms that contribute to the accumulation and programming of macrophages that maintain pain-associated behaviors in a mouse model of OA. We found that macrophages with an inflammatory phenotype accumulate in the lumbar DRG, innervating the damaged knee, early during OA development. These macrophages are not required for the initiation, but rather for the maintenance of OA pain, independent of the knee joint damage. Intriguingly, we identified myostatin is produced by sensory neurons, whilst CXCL11 appeared to be expressed by some satellite cells, and together contribute to the accumulation of F4/80$^+$iNOS$^+$ macrophages in the DRG of OA mice and regulate the maintenance of OA pain. Only intrathecal administration of myostatin, in naive mice was sufficient to increase F4/80$^+$iNOS$^+$ macrophages in the DRG and provoke pain-associated behaviors in a CXCL11-dependent manner. In contrast, CXCL11 contributes to the accumulation of total macrophages in the DRG, but was not sufficient to induce pain-associated behaviors. Therefore, we conclude that likely a range of factors contribute to neuron-macrophages communication in the maintenance of OA pain, where CXCL11 contributes the accumulation of DRG macrophages and together with myostatin plays and essential role in programming these macrophages into a pain maintaining pro-inflammatory phenotype. Finally, we identified that inhibition of myostatin may represent a novel unexpected therapeutic target for the treatment of chronic OA pain.

Different studies have pointed to DRG macrophages in the regulation of various pain conditions. DRG macrophages resolve inflammatory pain by transferring mitochondria to sensory neurons (van der Vlist et al., 2022). In contrast to a role in inflammatory pain resolution, DRG macrophages initiate and maintain neuropathic pain (Yu et al., 2020). More recently, OA was added to this list. The number of macrophages in the DRG is increased in different rodent models of OA (Miller et al., 2012; Raoof et al., 2021; Raoof, Willemen, & Eijkelkamp, 2018). Here, we identified that these macrophages are key for the maintenance of OA pain, whilst they are not needed for the initial development of pain induced by joint damage. This specific role of macrophages in only the maintenance of OA pain differs from that found in neuropathic pain, where DRG macrophages are required for the initiation and maintenance of neuropathic pain (Yu et al., 2020). This indicates that neuro-immune interactions may be pain condition-specific in the initiation phase, but the pain maintaining role of macrophages may be shared across pain conditions.

Macrophages depletion reduced pain-associated behaviors from day 3 onwards, whilst the number of macrophages, myostatin and CXCL11 are already increased at day 3 in the DRG. This questions what else than macrophages is driving pain at day 3 or earlier. Likely, knee tissue damage and the resulting DAMPS and inflammatory molecules cause pain-associated behaviors during the early phase of OA. As example, OA chondrocytes express cytokines, including IL-1β, TNF and TGFβ, that either directly or indirectly cause pain by activating nociceptors (Blaney Davidson et al., 2015; Manni et al., 2003; Melchiorri et al., 1998; Takano et al., 2019). In line with an inflammatory component driving pain, is that paracetamol and NSAIDs reduce pain at the first day of MIA-induced OA while at the later phase they do not (de Sousa Valente, 2019). Thus, inflammatory and tissue damage mediators in the joint likely cause pain at the early stage of OA (Vincent, 2020) by direct activation and sensitization of joint nociceptors independent of macrophages. Whether these early inflammatory triggers also engage the myostatin-CXCL11-macrophages axis in the DRG to maintain pain remains to be determined.

CXCL11 neutralization prevented the development of persistent OA pain, but intrathecal administration of CXCL11 was not sufficient to induce pain. CXCL11 is a well-known chemoattractant that activates CXCR3, CXCR4 and CXCR7, expressed on monocytes, neurons and glial cells (Bhangoo et al., 2007; Biber et al., 2002; Groom & Luster, 2011; Odemis et al., 2010; Oh et al., 2001; Shimizu et al., 2011; Singh et al., 2013). CXCR3 and CXCR4 are increased in the DRG in different rat models of neuropathic pain, and receptor antagonists reduced mechanical hypersensitivity in these models (Bhangoo et al., 2007; Chen et al., 2019). Although we did not verify receptor levels in our model, other studies in OA models (destabilization of the medial meniscus; mechanical joint loading) did not identify changes in CXCR3 and CXCR4 expression (Bangash et al., 2018; Miller et al., 2020). Different studies showed that spinal cord astrocytes express CXCL11 following spinal nerve injury (Guo et al., 2017; Piotrowska et al., 2018; Wu et al., 2018). Although we observed an increase in CXCL11 immunofluorescence in the DRG of mice with experimental OA that colocalized with some satellite glial cells markers, future work will need to assess whether satellite glial cells actually release CXCL11 or other cells may also express and release CXCL11, as not all CXCL11 immunofluorescence colocalized with satellite glial cells markers, and whether myostatin is a possible inducer of CXCL11. In line with our observations, CXCL11 is also upregulated relatively early, 2 days, after nerve damage, and blocking CXCR3 reduced allodynia in chronic constriction injury-induced rat model of neuropathic pain (Piotrowska et al., 2018). A study found that intrathecal injection of 400 ng of CXCL11 induced pain-associated behavior at 1.5 h after intrathecal injection (Piotrowska et al., 2018). We did not observe that a similar dose of intrathecal CXCL11 produced pain-associated behaviors at either 1 or 3 h after injection. Possibly CXCL11 only induces a very short episode of pain through direct actions on sensory neurons. The same study, however, did not observe CXCL11-induced allodynia 3 h after injection. Despite absence of pain behaviors at 24 h after injection, CXCL11 was sufficient to increase the number of macrophages in the DRG. Yet, macrophages did not acquire a pro-algesic F4/80$^+$iNOS$^+$ phenotype, possibly explaining why CXCL11 did not induce pain. In support of the requirement of F4/80$^+$iNOS$^+$ macrophages to induce pain, intrathecal injection of *in vitro* stimulated proinflammatory F4/80$^+$iNOS$^+$ macrophages, but not of unstimulated macrophages, into WT mice induces mechanical hypersensitivity (Raoof et al., 2021).

IL-6 and IL-18 were also in the top 4 list of increased factors in mice DRG during OA pain establishment. Although we did not focus on the two other proteins to test for their contribution, IL-6 is a classical cytokine expressed by pro-inflammatory macrophages (Qin et al., 2012). Moreover, there are several studies linking IL-6 protein production and mRNA expression in the DRG with pain (De Jongh et al., 2003). IL-18 has also been linked to inflammation, but requires cleavage from its precursor form (pro-IL-18) to its active form, which is initiated by NLRP3 inflammasome activation (van de Veerdonk et al., 2011). We recently identified a potential role of IL-18 and inflammasome activation in OA pain specifically in male mice (Ribeiro et al., 2023). Whether myostatin, CXCL11 and IL-18 are all required in concert remains to be determined.

In this study we identified a hitherto novel role of myostatin in

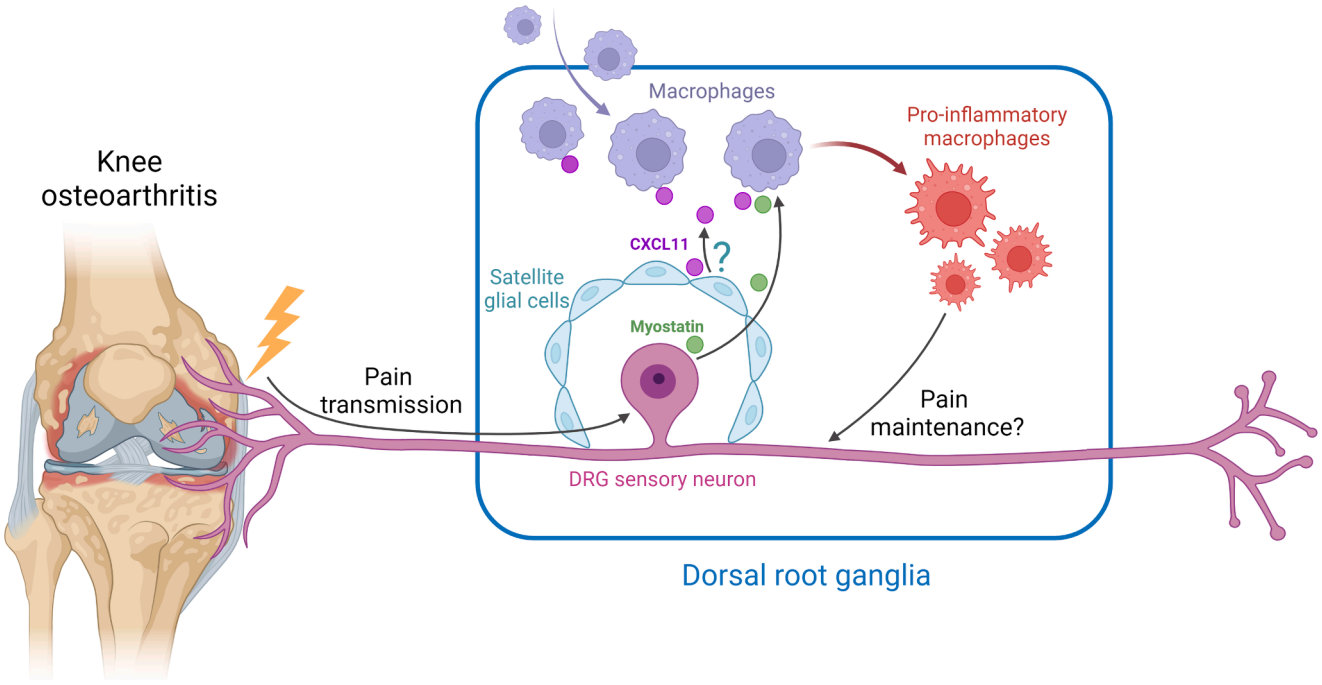

Fig. 6. Summary diagram. During OA, DRG sensory neurons produce myostatin, and CXCL11 is sequentially produced possibly by satellite glial cells. These factors contribute to the attraction and programming of DRG macrophages into a pro-algesic phenotype that maintains pain in OA.

promoting pro-algesic F4/80^{+}iNOS^{+} macrophages in the DRG and pain maintenance in OA. Myostatin is an extracellular cytokine member within the transforming growth factor-β (TGF-β) family and mostly expressed in skeletal muscles. It plays a crucial role in the negative regulation of muscle mass. Upon the binding to activin receptor type-2b (Acvr2b) (Lee & McPherron, 2001), myostatin initiates several different signaling cascades resulting in the upregulation of genes that promote iatrogenesis of muscles, whilst downregulating important myogenesis genes. Inhibition of myostatin, genetically or pharmacologically, with anti-myostatin antibody or propeptide, increases skeletal muscle mass (Camporez et al., 2016; Collins-Hooper et al., 2014; McPherron, Lawler, & Lee, 1997). Although its role in the sensory system has not been described, single cell RNAseq indicates that sets of sensory neurons express myostatin (Usoskin et al., 2015). Here we also confirmed that, during OA, sensory neurons innervating the affected joint but also other neurons express myostatin, with the largest increase in expression predominantly in small diameter neurons. But how does myostatin induce pain? Mice deficient in myostatin have decreased osteoclast numbers, increased cortical thickness, cortical tissue mineral density in the tibia, and increased vertebral bone mineral density (Omosule & Phillips, 2021). Additionally, there is some evidence that links myostatin with inflammation and macrophages infiltration and programming. Inhibition of myostatin reduced expression of TNF, IL-6 and F4/80 in muscles from mice with chronic kidney disease (Zhang et al., 2011) and obesity-induced insulin resistance (Dong et al., 2016; Wilkes, Lloyd, & Gekakis, 2009). Myostatin inhibition also suppresses macrophages infiltration in adipose tissue, while *in vitro* stimulation of macrophages with myostatin promoted IL-6 production (Dong et al., 2016). In line with these results, we observed that neutralization of myostatin during developing or established OA prevented accumulation of pro-inflammatory F4/80^{+}iNOS^{+} macrophages in the DRG. Furthermore, intrathecal myostatin administration increased the number of total and F4/80^{+}iNOS^{+} macrophages in the DRG. Therefore, myostatin's role regarding DRG macrophages appears not to be restricted to pro-inflammatory programming, but also to their accumulation. In line with these findings, we show that myostatin-induced pain-associated behaviors required CXCL11, possibly explaining as to how myostatin promotes macrophage accumulation. Overall, these findings extent the role of the cytokine myostatin beyond an immune regulator in adipose tissue, to one that involves neuro-immune communication in nervous tissues.

Despite the hitherto unknown role of myostatin in OA pain, we do not know whether myostatin directly programs macrophages into a pro-algesic F4/80^{+}iNOS^{+} macrophages, or whether this involves other cells present in the DRG. We show that macrophages stimulated with myostatin do not express the M1-like marker iNOS (Fig. S5), whilst classically stimulated macrophages with LPS and IFNγ do (Raoof et al., 2021). This would be in line with recent sequencing data of nervous tissue macrophages that shows that these cells hardly express activin receptor type-2a (Acvr2a) or Acvr2b. Possibly, myostatin-driven programming of DRG macrophages to pro-inflammatory phenotype requires an intermediate cell/factor. As examples, subsets of DRG neurons (e.g., neurofilament+ neurons, peptidergic and non-peptidergic neurons) and satellite glial cells, express Acvr2a, one of the receptors of myostatin (Jager et al., 2020; Usoskin et al., 2015). Possibly, myostatin only promotes an F4/80^{+}iNOS^{+} phenotype when expressed together with other inflammatory molecules such as CXCL11. The fact that neurons also express myostatin receptor Acvr2a may also explain why neutralization of myostatin has faster effects on pain-associated behaviors than macrophages depletion. Future research has to elucidate whether sensory-neuron derived myostatin acts on satellite glial cells to facilitate programming of macrophages into a pro-algesic state during OA.

A limitation of this study is that we did not assess whether the various treatments affected knee swelling and/or histology. However, most of the treatments were applied with intrathecal injection and were sufficient to reduce pain-associated behaviors. In addition, intrathecal injection of DT in MM^{dtr} mice only depleted macrophages in the DRG, not systemically, but was sufficient to reduce OA-induced mechanical hypersensitivity (Raoof et al., 2021). Therefore, we postulate that it is rather unlikely that our treatments targeting the myostain-CXCL11 axis have affected knee joint pathology.

Intrathecal treatments in this study target the DRG and spinal cord area, so it cannot be completely excluded that these treatments only affect the DRG and not the spinal cord. However, the increase of myostatin is observed in sensory neurons and CXCL11 in some extent in

satellite glial cells in the DRG, and neutralizing antibodies targeting these proteins reduced MIA-induced mechanical hypersensitivity. These observations suggest that treatment effects are peripherally driven.

Targeting myostatin has been a therapeutic strategy for some diseases associated with debilitating loss of musculoskeletal tissues. This has yielded in the development of myostatin inhibitors, ranging from natural antagonists to antibodies and soluble receptors (Suh & Lee, 2020). Some of these inhibitors, such as BYM-338, an anti-Acvr2b antibody, have been tested in Phase III trials to treat sarcopenia (Rooks et al., 2017) and chronic obstructive pulmonary disease (Polkey et al., 2019). Peptibody AMG-745, developed by Amgen, has been used in trials for treating patients receiving androgen deprivation therapy for prostate cancer (Padhi et al., 2014). Despite studies showed safety, clinical efficacy in various cases have been somewhat disappointing (Padhi et al., 2014; Polkey et al., 2019; Rooks et al., 2017; Rybalka et al., 2020). In this study we show that myostatin neutralizing antibodies resolve persistent OA pain, opening the possibility for a new use of these inhibitors. A limitation, however, is that we have only tested it in the mouse MIA-model of OA, which is a model with fast developing, and vigorous signs of cartilage damage and synovial inflammation. Given that OA is a slowly progressing disease, future research is needed to assess whether myostatin role in pain is consistent among other OA pain models.

4.1. Conclusion

We identified that CXCL11 and myostatin are ligands in neuron-to-macrophages communication in a preclinical model of OA (Fig. 6). CXCL11 drives the accumulation of DRG macrophages whilst myostatin predominantly programs DRG macrophages into pro-algesic inflammatory macrophages that maintain OA pain. These findings may explain clinical findings pointing that the severity of OA pain does not correlate well with the tissue changes in the injured joint. In addition, these findings point to completely novel potential therapeutic approaches to treat pain inOA, focused on preventing macrophage accumulation in nervous tissue or preventing their programming into pro-algesic phenotypes.

Authors contribution

Author contributions: Conceptualization: N.E., C.M.G. Investigation: C.M.G., R.R., S.V., H.L.D.M.W., N.E. Formal analysis: C.M.G., R.R. Visualization: C.M.G. Writing: C.M.G., N.E. Reviewing and editing, N.E., S.C.M., H.L.D.M.W. Supervision: N.E., S.C.M., F.P.J.G.L. Project administration: N.E. Funding acquisition: N.E., S.C.M., F.P.J.G.L.

Data availability

Data will be made available on request.

Acknowledgements

This work was supported by the European Union Horizon 2020 Research and Innovation Program under Marie Skłodowska-Curie Grants 642720 and 814244. F.P.J.G.L. and S.C.M. were supported by the Dutch Arthritis Association (Grant LLP-9). We thank Judith Prado for assistance with immunofluorescent imaging and analysis, Patricia Ribeiro for technical assistance with real-time RT-PCR, and Megan van Opstal for technical assistance with immunofluorescent stainings of DRG.

Appendix A. Supplementary data

Supplementary data to this article can be found online at https://doi.org/10.1016/j.bbi.2023.12.004.

References

Allen, K.D., Thoma, L.M., Golightly, Y.M., 2022. Epidemiology of osteoarthritis. Osteoarthritis Cartilage 30 (2), 184–195. https://doi.org/10.1016/j.joca.2021.04.020.

Bangash, M. A., Alles, S. R. A., Santana-Varela, S., Millet, Q., Sikandar, S., de Clauser, L., Ter Heegde, F., Habib, A. M., Pereira, V., Sexton, J. E., Emery, E. C., Li, S., Luiz, A. P., Erdos, J., Gossage, S. J., Zhao, J., Cox, J. J., & Wood, J. N. (2018). Distinct transcriptional responses of mouse sensory neurons in models of human chronic pain conditions. *Wellcome Open Res*, *3*, 78. 10.12688/wellcomeopenres.14641.1.

Bhangoo, S.K., Ren, D., Miller, R.J., Chan, D.M., Ripsch, M.S., Weiss, C., McGinnis, C., White, F.A., 2007. CXCR4 chemokine receptor signaling mediates pain hypersensitivity in association with antiretroviral toxic neuropathy. Brain Behav Immun 21 (5), 581–591. https://doi.org/10.1016/j.bbi.2006.12.003.

Biber, K., Dijkstra, I., Trebst, C., De Groot, C.J., Ransohoff, R.M., Boddeke, H.W., 2002. Functional expression of CXCR3 in cultured mouse and human astrocytes and microglia. Neuroscience 112 (3), 487–497. https://doi.org/10.1016/s0306-4522(02)00114-8.

Bijlsma, J.W., Berenbaum, F., Lafeber, F.P., 2011. Osteoarthritis: an update with relevance for clinical practice. Lancet 377 (9783), 2115–2126. https://doi.org/10.1016/S0140-6736(11)60243-2.

Blaney Davidson, E.N., van Caam, A.P., Vitters, E.L., Bennink, M.B., Thijssen, E., van den Berg, W.B., Koenders, M.I., van Lent, P.L., van de Loo, F.A., van der Kraan, P.M., 2015. TGF-beta is a potent inducer of Nerve Growth Factor in articular cartilage via the ALK5-Smad2/3 pathway. Potential role in OA related pain? Osteoarthritis Cartilage 23 (3), 478–486. https://doi.org/10.1016/j.joca.2014.12.005.

Camporez, J.P., Petersen, M.C., Abudukadier, A., Moreira, G.V., Jurczak, M.J., Friedman, G., Haqq, C.M., Petersen, K.F., Shulman, G.I., 2016. Anti-myostatin antibody increases muscle mass and strength and improves insulin sensitivity in old mice. Proc Natl Acad Sci U S A 113 (8), 2212–2217. https://doi.org/10.1073/pnas.1525795113.

Chen, Y., Yin, D., Fan, B., Zhu, X., Chen, Q., Li, Y., Zhu, S., Lu, R., Xu, Z., 2019. Chemokine CXCL10/CXCR3 signaling contributes to neuropathic pain in spinal cord and dorsal root ganglia after chronic constriction injury in rats. Neurosci Lett 694, 20–28. https://doi.org/10.1016/j.neulet.2018.11.021.

Collins-Hooper, H., Sartori, R., Macharia, R., Visanuvimol, K., Foster, K., Matsakas, A., Flasskamp, H., Ray, S., Dash, P.R., Sandri, M., Patel, K., 2014. Propeptide-mediated inhibition of myostatin increases muscle mass through inhibiting proteolytic pathways in aged mice. J Gerontol A Biol Sci Med Sci 69 (9), 1049–1059. https://doi.org/10.1093/gerona/glt170.

De Jongh, R.F., Vissers, K.C., Meert, T.F., Booij, L., De Deyne, C.S., Heylen, R.J., 2003. The role of interleukin-6 in nociception and pain. Anesth Analg 96 (4), 1096–1103. https://doi.org/10.1213/01.ANE.0000055362.56604.78.

de Sousa Valente, J., 2019. The Pharmacology of Pain Associated With the Monoiodoacetate Model of Osteoarthritis. Front Pharmacol 10, 974. https://doi.org/10.3389/fphar.2019.00974.

Dong, J., Dong, Y., Dong, Y., Chen, F., Mitch, W.E., Zhang, L., 2016. Inhibition of myostatin in mice improves insulin sensitivity via irisin-mediated cross talk between muscle and adipose tissues. Int J Obes (lond) 40 (3), 434–442. https://doi.org/10.1038/ijo.2015.200.

Eijkelkamp, N., Heijnen, C.J., Willemen, H.L., Deumens, R., Joosten, E.A., Kleibeuker, W., den Hartog, I.J., van Velthoven, C.T., Nijboer, C., Nassar, M.A., Dorn 2nd, G.W., Wood, J.N., Kavelaars, A., 2010. GRK2: a novel cell-specific regulator of severity and duration of inflammatory pain. J Neurosci 30 (6), 2138–2149. https://doi.org/10.1523/JNEUROSCI.5752-09.2010.

Fingleton, C., Smart, K., Moloney, N., Fullen, B.M., Doody, C., 2015. Pain sensitization in people with knee osteoarthritis: a systematic review and meta-analysis. Osteoarthritis Cartilage 23 (7), 1043–1056. https://doi.org/10.1016/j.joca.2015.02.163.

Groom, J.R., Luster, A.D., 2011. CXCR3 in T cell function. Exp Cell Res 317 (5), 620–631. https://doi.org/10.1016/j.yexcr.2010.12.017.

Guo, G., Peng, Y., Xiong, B., Liu, D., Bu, H., Tian, X., Yang, H., Wu, Z., Cao, F., Gao, F., 2017. Involvement of chemokine CXCL11 in the development of morphine tolerance in rats with cancer-induced bone pain. J Neurochem 141 (4), 553–564. https://doi.org/10.1111/jnc.13919.

Gwilym, S.E., Keltner, J.R., Warnaby, C.E., Carr, A.J., Chizh, B., Chessell, I., Tracey, I., 2009. Psychophysical and functional imaging evidence supporting the presence of central sensitization in a cohort of osteoarthritis patients. Arthritis Rheum 61 (9), 1226–1234. https://doi.org/10.1002/art.24837.

Hylden, J.L., Wilcox, G.L., 1980. Intrathecal morphine in mice: a new technique. Eur J Pharmacol 67 (2–3), 313–316. https://doi.org/10.1016/0014-2999(80)90515-4.

Jager, S.E., Pallesen, L.T., Richner, M., Harley, P., Hore, Z., McMahon, S., Denk, F., Vaegter, C.B., 2020. Changes in the transcriptional fingerprint of satellite glial cells following peripheral nerve injury. Glia 68 (7), 1375–1395. https://doi.org/10.1002/glia.23785.

Lee, S.J., McPherron, A.C., 2001. Regulation of myostatin activity and muscle growth. Proc Natl Acad Sci U S A 98 (16), 9306–9311. https://doi.org/10.1073/pnas.151270098.

Lluch, E., Nijs, J., Courtney, C.A., Rebbeck, T., Wylde, V., Baert, I., Wideman, T.H., Howells, N., Skou, S.T., 2018. Clinical descriptors for the recognition of central sensitization pain in patients with knee osteoarthritis. Disabil Rehabil 40 (23), 2836–2845. https://doi.org/10.1080/09638288.2017.1358770.

Manni, L., Lundeberg, T., Fiorito, S., Bonini, S., Vigneti, E., Aloe, L., 2003. Nerve growth factor release by human synovial fibroblasts prior to and following exposure to tumor necrosis factor-alpha, interleukin-1 beta and cholecystokinin-8: the possible

role of NGF in the inflammatory response. Clin Exp Rheumatol 21 (5), 617–624. https://www.ncbi.nlm.nih.gov/pubmed/14611111.
McPherron, A.C., Lawler, A.M., Lee, S.J., 1997. Regulation of skeletal muscle mass in mice by a new TGF-beta superfamily member. Nature 387 (6628), 83–90. https://doi.org/10.1038/387083a0.
Melchiorri, C., Meliconi, R., Frizziero, L., Silvestri, T., Pulsatelli, L., Mazzetti, I., Borzi, R. M., Uguccioni, M., Facchini, A., 1998. Enhanced and coordinated in vivo expression of inflammatory cytokines and nitric oxide synthase by chondrocytes from patients with osteoarthritis. Arthritis Rheum 41 (12), 2165–2174. https://doi.org/10.1002/1529-0131(199812)41:12<2165::AID-ART11>3.0.CO;2-O.
Miller, R.E., Tran, P.B., Das, R., Ghoreishi-Haack, N., Ren, D., Miller, R.J., Malfait, A.M., 2012. CCR2 chemokine receptor signaling mediates pain in experimental osteoarthritis. Proc Natl Acad Sci U S A 109 (50), 20602–20607. https://doi.org/10.1073/pnas.1209294110.
Miller, R.E., Tran, P.B., Ishihara, S., Syx, D., Ren, D., Miller, R.J., Valdes, A.M., Malfait, A. M., 2020. Microarray analyses of the dorsal root ganglia support a role for innate neuro-immune pathways in persistent pain in experimental osteoarthritis. Osteoarthritis Cartilage 28 (5), 581–592. https://doi.org/10.1016/j.joca.2020.01.008.
Neogi, T., 2013. The epidemiology and impact of pain in osteoarthritis. Osteoarthritis Cartilage 21 (9), 1145–1153. https://doi.org/10.1016/j.joca.2013.03.018.
Odemis, V., Boosmann, K., Heinen, A., Kury, P., Engele, J., 2010. CXCR7 is an active component of SDF-1 signalling in astrocytes and Schwann cells. J Cell Sci 123 (Pt 7), 1081–1088. https://doi.org/10.1242/jcs.062810.
Oh, S.B., Tran, P.B., Gillard, S.E., Hurley, R.W., Hammond, D.L., Miller, R.J., 2001. Chemokines and glycoprotein120 produce pain hypersensitivity by directly exciting primary nociceptive neurons. J Neurosci 21 (14), 5027–5035. https://doi.org/10.1523/JNEUROSCI.21-14-05027.2001.
Omosule, C.L., Phillips, C.L., 2021. Deciphering Myostatin's Regulatory, Metabolic, and Developmental Influence in Skeletal Diseases. Front Genet 12, 662908. https://doi.org/10.3389/fgene.2021.662908.
Ostojic, M., Ostojic, M., Prlic, J., Soljic, V., 2019. Correlation of anxiety and chronic pain to grade of synovitis in patients with knee osteoarthritis. Psychiatr Danub 31 (Suppl 1), 126–130. https://www.ncbi.nlm.nih.gov/pubmed/30946731.
Padhi, D., Higano, C.S., Shore, N.D., Sieber, P., Rasmussen, E., Smith, M.R., 2014. Pharmacological inhibition of myostatin and changes in lean body mass and lower extremity muscle size in patients receiving androgen deprivation therapy for prostate cancer. J Clin Endocrinol Metab 99 (10), E1967–E1975. https://doi.org/10.1210/jc.2014-1271.
Pinto, M., Lima, D., Tavares, I., 2007. Neuronal activation at the spinal cord and medullary pain control centers after joint stimulation: a c-fos study in acute and chronic articular inflammation. Neuroscience 147 (4), 1076–1089. https://doi.org/10.1016/j.neuroscience.2007.05.019.
Piotrowska, A., Rojewska, E., Pawlik, K., Kreiner, G., Ciechanowska, A., Makuch, W., Zychowska, M., Mika, J., 2018. Pharmacological blockade of CXCR3 by (+/-)-NBI-74330 reduces neuropathic pain and enhances opioid effectiveness - Evidence from in vivo and in vitro studies. Biochim Biophys Acta Mol Basis Dis 1864 (10), 3418–3437. https://doi.org/10.1016/j.bbadis.2018.07.032.
Pitcher, T., Sousa-Valente, J., Malcangio, M., 2016. The Monoiodoacetate Model of Osteoarthritis Pain in the Mouse. J vis Exp(111). https://doi.org/10.3791/53746.
Polkey, M.I., Praestgaard, J., Berwick, A., Franssen, F.M.E., Singh, D., Steiner, M.C., Casaburi, R., Tillmann, H.C., Lach-Trifilieff, E., Roubenoff, R., Rooks, D.S., 2019. Activin Type II Receptor Blockade for Treatment of Muscle Depletion in Chronic Obstructive Pulmonary Disease. A Randomized Trial. Am J Respir Crit Care Med 199 (3), 313–320. https://doi.org/10.1164/rccm.201802-0286OC.
Qin, H., Holdbrooks, A.T., Liu, Y., Reynolds, S.L., Yanagisawa, L.L., Benveniste, E.N., 2012. SOCS3 deficiency promotes M1 macrophage polarization and inflammation. J Immunol 189 (7), 3439–3448. https://doi.org/10.4049/jimmunol.1201168.
Raoof, R., Willemen, H., Eijkelkamp, N., 2018. Divergent roles of immune cells and their mediators in pain. Rheumatology (oxford) 57 (3), 429–440. https://doi.org/10.1093/rheumatology/kex308.
Raoof, R., Martin Gil, C., Lafeber, F., de Visser, H., Prado, J., Versteeg, S., Pascha, M.N., Heinemans, A.L.P., Adolfs, Y., Pasterkamp, J., Wood, J.N., Mastbergen, S.C., Eijkelkamp, N., 2021. Dorsal Root Ganglia Macrophages Maintain Osteoarthritis Pain. J Neurosci 41 (39), 8249–8261. https://doi.org/10.1523/JNEUROSCI.1787-20.2021.
Rooks, D.S., Laurent, D., Praestgaard, J., Rasmussen, S., Bartlett, M., Tanko, L.B., 2017. Effect of bimagrumab on thigh muscle volume and composition in men with casting-induced atrophy. J Cachexia Sarcopenia Muscle 8 (5), 727–734. https://doi.org/10.1002/jcsm.12205.
Rybalka, E., Timpani, C.A., Debruin, D.A., Bagaric, R.M., Campelj, D.G., Hayes, A., 2020. The Failed Clinical Story of Myostatin Inhibitors against Duchenne Muscular Dystrophy: Exploring the Biology behind the Battle. Cells 9 (12). https://doi.org/10.3390/cells9122657.
Safiri, S., Kolahi, A.A., Smith, E., Hill, C., Bettampadi, D., Mansournia, M.A., Hoy, D., Ashrafi-Asgarabad, A., Sepidarkish, M., Almasi-Hashiani, A., Collins, G., Kaufman, J., Qorbani, M., Moradi-Lakeh, M., Woolf, A.D., Guillemin, F., March, L., Cross, M., 2020. Global, regional and national burden of osteoarthritis 1990–2017: a systematic analysis of the Global Burden of Disease Study 2017. Ann Rheum Dis 79 (6), 819–828. https://doi.org/10.1136/annrheumdis-2019-216515.
Schreiber, H.A., Loschko, J., Karssemeijer, R.A., Escolano, A., Meredith, M.M., Mucida, D., Guermonprez, P., Nussenzweig, M.C., 2013. Intestinal monocytes and macrophages are required for T cell polarization in response to Citrobacter rodentium. J Exp Med 210 (10), 2025–2039. https://doi.org/10.1084/jem.20130903.
Shimizu, S., Brown, M., Sengupta, R., Penfold, M.E., Meucci, O., 2011. CXCR7 protein expression in human adult brain and differentiated neurons. PLoS One 6 (5), e20680.
Silva Santos Ribeiro P, Willemen HLDM, Versteeg S, Martin Gil C, Eijkelkamp N. NLRP3 inflammasome activation in sensory neurons promotes chronic inflammatory and osteoarthritis pain. Immunother Adv. 2023 Oct 24;3(1):ltad022. doi: 10.1093/immadv/ltad022. PMID: 38047118; PMCID: PMC10691442.
Simeoli, R., Montague, K., Jones, H.R., Castaldi, L., Chambers, D., Kelleher, J.H., Vacca, V., Pitcher, T., Grist, J., Al-Ahdal, H., Wong, L.F., Perretti, M., Lai, J., Mouritzen, P., Heppenstall, P., Malcangio, M., 2017. Exosomal cargo including microRNA regulates sensory neuron to macrophage communication after nerve trauma. Nat Commun 8 (1), 1778. https://doi.org/10.1038/s41467-017-01841-5.
Singh, A.K., Arya, R.K., Trivedi, A.K., Sanyal, S., Baral, R., Dormond, O., Briscoe, D.M., Datta, D., 2013. Chemokine receptor trio: CXCR3, CXCR4 and CXCR7 crosstalk via CXCL11 and CXCL12. Cytokine Growth Factor Rev 24 (1), 41–49. https://doi.org/10.1016/j.cytogfr.2012.08.007.
Steen Pettersen, P., Neogi, T., Magnusson, K., Berner Hammer, H., Uhlig, T., Kvien, T.K., Haugen, I.K., 2019. Peripheral and Central Sensitization of Pain in Individuals With Hand Osteoarthritis and Associations With Self-Reported Pain Severity. Arthritis Rheumatol 71 (7), 1070–1077. https://doi.org/10.1002/art.40850.
Suh, J., & Lee, Y. S. (2020). Myostatin Inhibitors: Panacea or Predicament for Musculoskeletal Disorders? *J Bone Metab*, *27*(3), 151-165. 10.11005/jbm.2020.27.3.151.
Suzuki, S., Awaya, G., Wakita, S., Maekawa, M., Ikeda, T., 1987. Diagnosis by ultrasound of congenital dislocation of the hip joint. Clin Orthop Relat Res(217), 171–178. https://www.ncbi.nlm.nih.gov/pubmed/3549090.
Takano, S., Uchida, K., Itakura, M., Iwase, D., Aikawa, J., Inoue, G., Mukai, M., Miyagi, M., Murata, K., Sekiguchi, H., Takaso, M., 2019. Transforming growth factor-beta stimulates nerve growth factor production in osteoarthritic synovium. BMC Musculoskelet Disord 20 (1), 204. https://doi.org/10.1186/s12891-019-2595-z.
Trouvin, A.P., Perrot, S., 2018. Pain in osteoarthritis. Implications for optimal management. Joint Bone Spine 85 (4), 429–434. https://doi.org/10.1016/j.jbspin.2017.08.002.
Usoskin, D., Furlan, A., Islam, S., Abdo, H., Lonnerberg, P., Lou, D., Hjerling-Leffler, J., Haeggstrom, J., Kharchenko, O., Kharchenko, P.V., Linnarsson, S., Ernfors, P., 2015. Unbiased classification of sensory neuron types by large-scale single-cell RNA sequencing. Nat Neurosci 18 (1), 145–153. https://doi.org/10.1038/nn.3881.
van de Veerdonk, F.L., Netea, M.G., Dinarello, C.A., Joosten, L.A., 2011. Inflammasome activation and IL-1beta and IL-18 processing during infection. Trends Immunol 32 (3), 110–116. https://doi.org/10.1016/j.it.2011.01.003.
van der Vlist, M., Raoof, R., Willemen, H., Prado, J., Versteeg, S., Martin Gil, C., Vos, M., Lokhorst, R.E., Pasterkamp, R.J., Kojima, T., Karasuyama, H., Khoury-Hanold, W., Meyaard, L., Eijkelkamp, N., 2022. Macrophages transfer mitochondria to sensory neurons to resolve inflammatory pain. Neuron 110 (4), 613–626 e619. https://doi.org/10.1016/j.neuron.2021.11.020.
van Helvoort, E.M., Welsing, P.M.J., Jansen, M.P., Gielis, W.P., Loef, M., Kloppenburg, M., Blanco, F., Haugen, I.K., Berenbaum, F., Bay-Jensen, A.C., Ladel, C., Lalande, A., Larkin, J., Loughlin, J., Mobasheri, A., Weinans, H., Lafeber, F., Eijkelkamp, N., Mastbergen, S., 2021. Neuropathic pain in the IMI-APPROACH knee osteoarthritis cohort: prevalence and phenotyping. RMD Open 7 (3). https://doi.org/10.1136/rmdopen-2021-002025.
Vincent, T.L., 2020. Peripheral pain mechanisms in osteoarthritis. Pain 161 Suppl 1(1), S138–S146. https://doi.org/10.1097/j.pain.0000000000001923.
Wilkes, J.J., Lloyd, D.J., Gekakis, N., 2009. Loss-of-function mutation in myostatin reduces tumor necrosis factor alpha production and protects liver against obesity-induced insulin resistance. Diabetes 58 (5), 1133–1143. https://doi.org/10.2337/db08-0245.
Wu, X.B., He, L.N., Jiang, B.C., Shi, H., Bai, X.Q., Zhang, W.W., Gao, Y.J., 2018. Spinal CXCL9 and CXCL11 are not involved in neuropathic pain despite an upregulation in the spinal cord following spinal nerve injury. Mol Pain 14, 1744806918777401. https://doi.org/10.1177/1744806918777401.
Wylde, V., Hewlett, S., Learmonth, I.D., Dieppe, P., 2011. Persistent pain after joint replacement: prevalence, sensory qualities, and postoperative determinants. Pain 152 (3), 566–572. https://doi.org/10.1016/j.pain.2010.11.023.
Yu, X., Liu, H., Hamel, K.A., Morvan, M.G., Yu, S., Leff, J., Guan, Z., Braz, J.M., Basbaum, A.I., 2020. Dorsal root ganglion macrophages contribute to both the initiation and persistence of neuropathic pain. Nat Commun 11 (1), 264. https://doi.org/10.1038/s41467-019-13839-2.
Zeng, Y.J., Lai, W., Wu, H., Liu, L., Xu, H.Y., Wang, J., Chu, Z.H., 2016. Neuroendocrine-like cells -derived CXCL10 and CXCL11 induce the infiltration of tumor-associated macrophage leading to the poor prognosis of colorectal cancer. Oncotarget 7 (19), 27394–27407. https://doi.org/10.18632/oncotarget.8423.
Zhang, L., Rajan, V., Lin, E., Hu, Z., Han, H.Q., Zhou, X., Song, Y., Min, H., Wang, X., Du, J., Mitch, W.E., 2011. Pharmacological inhibition of myostatin suppresses systemic inflammation and muscle atrophy in mice with chronic kidney disease. FASEB J 25 (5), 1653–1663. https://doi.org/10.1096/fj.10-176917.